A Design Method of the Rotor Auxiliary Slot for the Water-filled Submersible Induction Motors

Jiaxin Li, Jingwen Yan, Chong Di, Xiaohua Bao, *Member, IEEE*, and Qinglong Zhu

***Abstract*—Aiming at the problem of electromagnetic vibration of the water-filled submersible induction motor (WSIM), a method of opening auxiliary slots on the rotor side is proposed to weaken the air-gap field harmonics caused by the rotor slot permeance harmonics. By analyzing the research status of electromagnetic vibration of the WSIM and the composition of the air-gap magnetic field of the motor, the idea that the auxiliary slots mainly affect the air-gap field harmonics by changing the air-gap permeance of the motor is put forward. The mathematical model of air-gap permeance of WSIM is established to simulate the influence of auxiliary slots on the air-gap permeance. Through the parametric analysis of the mathematical model, the change of auxiliary slot size is simulated. The air-gap permeance waveform is decomposed by the two-dimensional Fourier transform, and then the variation of the air-gap permeance harmonics with the size of the auxiliary slot is analyzed. Finally, the finite element simulation model of the WSIM with the auxiliary slots is established, and the waveform of the air-gap flux density of the motor is analyzed to verify the effectiveness of the mathematical model. Meanwhile, the results show that after opening the auxiliary slot, the radial electromagnetic force of the motor was reduced by 28.4%.**

***Index Terms*—Auxiliary slot, the radial electromagnetic force, the Water-filled Submersible Induction Motors.**

I. INTRODUCTION

INDUCTION MOTORS are widely used in all walks of life, such as pumps, compressors, ventilation equipment, electric vehicles, washing machines, robots, and so on, because of their advantages of low manufacturing cost, stable structure, mature technology, and reliable operation. At the same time, the vibration and noise of motor seriously interfere with people's production and life, so how to suppress the electromagnetic noise and vibration has been a long-term and in-depth research topic[1].

As early as the 1950s, American scholars greatly simplified the motor model and conducted theoretical studies on stator natural frequency, radial force wave of the motor magnetic field, and vibration characteristics of the motor systematically [2].On these basics, scholars have done a lot of research on the analysis and prediction of electromagnetic vibration. In 1981, Yang Shijun of Heriot-Watt University in the UK further pointed out that one of the main sources of motor vibration is the radial electromagnetic force wave in the electromagnetic force wave, and analyzed the frequency component of the radial force wave through mathematical expression and experimental verification [3].Feng Chai et al. studied the relationship between air-gap deformation and electromagnetic performance and radial vibration characteristics of permanent magnet synchronous motor. At the same time, the speed of the motor was controlled as peak speed, and the output power was rated power [4]. Defeng Kong et al. mainly simulated the electromagnetic vibration caused by the electromagnetic forces under different loads and analyzed the causes of the electromagnetic vibration under different working conditions, respectively [5]. Sabin Sathyan et al. presented a new method of calculating the motor electromagnetic force. Firstly solve the node force by using the virtual work method and then use the nodes to solve the electromagnetic force of the motor. Finally, the effectiveness of the method is demonstrated by comparing the electromagnetic force calculated by this method with that actually measured [6]. In order to predict the radial vibration of switched reluctance motor when the motor is saturation, X. Guo al. proposed an improved model by using the improved Least Square Support Vector Machine [7].

With the development and wide application of inverters, more and more scholars turn their attention to the electromagnetic noise generated by the stator current harmonics generated by PWM inverters. Dong Jiang et al. analyzed the common-mode noise of the three-phase motor controller, which was caused by the high-frequency common-mode voltage and the common-mode conducted loop. Then they put forward an optimal PWM method which applied for advanced topologies, which improves the problem of excessive noise [8]. A. C. Binojkumar et al. presents an experimental procedure to determine the acoustic and vibration behavior of an inverter-fed induction motor based on measurements of the current spectrum, acoustic noise spectrum, overall noise in dB and overall A-weighted noise in dBA [9].

Manuscript received February 15, 2022; revised March 02, 2022; accepted March 09, 2022. date of publication March 25, 2022; date of current version March 18, 2022.

This work was supported by the National Natural Science Funds of China No. 51977055 and Major Science and Technology program of Anhui province No. 201903a05020042 and Anhui Province key laboratory of Large-scale Submersible Electric Pump and Accoutrements.

Jiaxin Li, Jingwen Yan, Chong Di, and Xiaohua Bao (*Corresponding Author*) are with the School of Electrical Engineering and Automation, Hefei University of Technology, Hefei, 230009 China (e-mail: 13721058410@163.com; 2019170308@hfut.edu.cn; baoxh@hfut.edu.cn; Chong.Di@hfut.edu.cn;).

Qinglong Zhu is with Hefei Hengda Jianghai Pump Co., Ltd, Hefei, 230000 China (e-mail: zhuqinglong@hdjh.cn).

(Corresponding Author: Xiaohua Bao)

Digital Object Identifier 10.30941/CESTEMS.2022.00006

And they also studied the electromagnetic noise of the motor driven by the variable switching frequency PWM method, and the results show that the frequency conversion PWM can reduce the line current THD at high speed [10]. H. Amlinger et al. quantitatively analyzed the influence of the switching frequency of the converter on the electromagnetic noise of the traction motor [11].

Scholars have also done a lot of work to reduce the electromagnetic noise of the motor caused by the spatial magnetomotive force harmonics and permeance harmonics. Yang Lu et al. analyzed the electromagnetic force and the vibration behavior of the axial flux permanent magnet synchronous machine and the permanent magnet auxiliary synchronous reluctance machine in detail. Then, an analytical method for calculating radial force based on the Maxwell stress tensor method is proposed, and a new type of separated winding is proposed, which can effectively alleviate the vibration of a double three-phase axial flux permanent magnet synchronous machine [12]- [13]. Nevertheless, it will complicate the WSIM winding installation process. The use of the rectangular wire windings can also reduce electromagnetic noise but are not suitable for the closed slot structure of WSIM [14]. Guiyu Zhou et al. Proposed a method of slotting on the surface of induction motor rotor core to reduce noise. In essence, the electromagnetic noise is reduced by suppressing the vibration caused by the magnetic conduction harmonic of the rotor slot. Finally, the effectiveness of the method is verified by comparing the experimental results of the prototype with the simulation results. [15]. However, slotting on the rotor surface will increase the water friction loss.

The method by slotting inside the rotor is used in this paper to reduce vibration and electromagnetic noise. And a new design method was put forward to optimize the size of the auxiliary slots. This paper first describes the composition of the air-gap field and analyzes the principle of optimizing the air-gap field harmonics by the auxiliary slot. Then the mathematical model of air-gap permeability is established, which is used to parameterize the influence of the auxiliary slots on the air-gap permeability. Finally, the effectiveness of the method is verified by finite element analysis. The THD of the air-gap permeance waveform and radial force of the motor is calculated. Also, the effect of the auxiliary slot is also analyzed.

II. Effect of Auxiliary Slot on Air-Gap Magnetic Field of WSIM

The slot numbers of the induction motor determine the distribution of magnetic flux density and radial electromagnetic force wave in the air-gap of the motor. Sensible choice of the slot numbers and the addition of auxiliary slots can weaken the electromagnetic noise related to the electromagnetic vibration.

This paper takes WSIM as the main research object, which is researched by many authors[16]-[20]. In higher power ranges of the water-filled submersible induction motors, the rotor widely uses a copper bar rotor which has closed slots. The closed slots can reduce the water friction loss of the motor, and the copper bar rotor can reduce the rotor copper loss. These lead to a large tooth area and low magnetic density of submersible motor rotor. At the same time, because the rotor surface slot will increase the water friction loss, we choose to slot inside the rotor.

A. Characterization of Air-Gap Magnetic Field

In order to calculate and reduce the electromagnetic vibration and noise, it is necessary to understand the source of radial electromagnetic force wave firstly, that is, to analyze the current distribution of the stator and the rotor. Then, we also need to analyze the influence of the stator slots and the rotor slots on air-gap permeance and the magnetomotive force. The air-gap magnetic density is equal to the product of magnetic potential and magnetic conductivity [15].

When the influence of core saturation on the motor is ignored, the radial air-gap magnetic density can be written as

$$b_r(\theta,t) = f(\theta,t)\lambda(\theta,t) \tag{1}$$

where $f(\theta, t)$ is the air-gap magnetomotive force, and $\lambda(\theta,\ t)$ is the air-gap permeance.

To simplify the analysis, it is assumed that the motor is powered by the source, which waveform is sinusoidal. Under the normal operation of the motor, the synthetic magnetomotive force of the stator and rotor winding can be expressed as

$$f(\theta,t) = f_0(\theta,t) + \sum_{\upsilon} f_\upsilon(\theta,t) + \sum_{\mu} f_\mu(\theta,t) \tag{2}$$

The first term in (2) is the fundamental magnetomotive force, and the second and third terms are the slot magnetomotive force harmonics produced by the currents of the stator and rotor, which can be described as

$$f_0(\theta,t) = F_0\cos(p\theta - \omega_1 t - \varphi_0) \tag{3}$$

$$f_\upsilon(\theta,t) = F_\upsilon\cos(\upsilon\theta - \omega_1 t - \varphi_1) \tag{4}$$

$$f_\mu(\theta,t) = F_\mu\cos(\mu\theta - \omega_\mu t - \varphi_2) \tag{5}$$

where p is the number of pole pairs, ω_1 is the rotation speed of the fundamental magnetomotive force of the stator, and ω_μ is the harmonic angular speed of the μth magnetomotive force of the rotor.

μ and υ are the pole pair of harmonics. For a three-phase induction motor with the stator slots number of Z_s and the rotor slots number of Z_r, there are

$$\upsilon = q_s Z_s + p \quad q_s = \pm 1,\ \pm 2,\ \ldots \tag{6}$$

$$\mu = q_r Z_r + p \quad q_r = \pm 1,\ \pm 2,\ \ldots \tag{7}$$

F_0, F_υ, F_μ in (3)- (5) can be expressed as

$$F_0 = 1.35\frac{W_1 K_{dp1}}{p} I_0 \tag{8}$$

$$F_\upsilon = 1.35\frac{W_1 K_{dp\upsilon}}{\upsilon} I_1 D_{2\upsilon} \tag{9}$$

$$F_\mu = 1.35\frac{W_1 K_{dp1}}{\mu} I_2' \tag{10}$$

where W_1 is the number of series turns of the stator and $K_{dp\upsilon}$ and K_{dp1} are the coefficients of the winding, $D_{2\upsilon}$ is the damping coefficient.

The air-gap permeance $\lambda(\theta,\ t)$ is mainly affected by the slotting of stator and rotor, which can be approximately

expressed as

$$\lambda(\theta,t)=\Lambda_0(1+\frac{\sum_{k_1}\lambda_{k_1}}{\Lambda_0})(1+\frac{\sum_{k_2}\lambda_{k_2}}{\Lambda_0}) \approx \Lambda_0+\sum_{k_1}\lambda_{k_1}+\sum_{k_2}\lambda_{k_2}+\sum_{k_1}\sum_{k_2}\lambda_{k_1k_2} \tag{11}$$

$$\Lambda_0=\frac{\mu_0}{\delta K_c} \tag{12}$$

$$\lambda_{k1}=\Lambda_{k1}\cos k_1 Z_1\theta \quad k_1=1,2,3,... \tag{13}$$

$$\lambda_{k2}=\Lambda_{k2}\cos k_2 Z_r[\theta-\frac{\omega}{p}(1-s)t] \quad k_2=1,2,3,... \tag{14}$$

$$\Lambda_{k1}=-\Lambda_0(-1)^{k_1}(K_{c1}-1)\left|\frac{\sin k_1\frac{K_{c1}-1}{K_{c1}}\pi}{k_1\frac{K_{c1}-1}{K_{c1}}\pi}\right| \tag{15}$$

$$\Lambda_{k2}=-\Lambda_0(-1)^{k_2}(K_{c2}-1)\left|\frac{\sin k_2\frac{K_{c2}-1}{K_{c2}}\pi}{k_2\frac{K_{c2}-1}{K_{c2}}\pi}\right| \tag{16}$$

where Λ_0 is the invariable part of air-gap permeance, λ_{k1} is the harmonic permeance when the rotor is smooth, and the stator is slotted, and λ_{k2} is the harmonic permeance when the stator is smooth, and the rotor is slotted, Λ_{k1} and Λ_{k2} are the amplitudes of permeance harmonics because of the opening of stator and rotor slots, respectively.

$$K_{c1}=\frac{t_1}{t_1-\Upsilon_1\delta} \tag{17}$$

$$\Upsilon_1=\frac{4}{\pi}[(\frac{b_{01}}{2\delta})tg^{-1}(\frac{b_{01}}{2\delta})-\ln\sqrt{1+(\frac{b_{01}}{2\delta})^2}] \tag{18}$$

where K_{c1} is Carter's coefficient when the rotor is smoothing and the stator is slotting. When the stator is smooth and the rotor slot, K_{c2} is obtained by replacing t_1 and b_{01} in (17) and (18) with t_2 and b_{02}, respectively. Where t_1 is the stator tooth distance, t_2 is the rotor tooth distance, b_{01} is the stator slot opening width, b_{02} is the rotor slot opening width.

By introducing equations (2)-(14) into (1) and neglecting some small amplitude components, the radial air-gap magnetic field $b(\theta, t)$ can be rewritten as

$$\begin{aligned} b_r(\theta,t) \approx & F_0\Lambda_0\cos(p\theta-\omega_1 t-\varphi_{0r}) \\ & +\sum_{\upsilon}F_\upsilon\Lambda_0\cos(\upsilon\theta-\omega_1 t-\varphi_1) \\ & +\sum_{\mu}F_\mu\Lambda_0\cos(\mu\theta-\omega_\mu t-\varphi_2) \\ & +\sum_{\upsilon}\frac{F_0}{2}\Lambda_{k1}\cos(\upsilon\theta-\omega_1 t-\varphi_{0r}) \\ & +\sum_{\mu}\frac{F_0}{2}\Lambda_{k2}\cos(\mu\theta-\omega_\mu t-\varphi_{0r}) \end{aligned} \tag{19}$$

The first polynomial at the right hand of equation (19) is the expression of the fundamental air-gap magnetic field. The second polynomial and the third polynomial are the air-gap field harmonics caused by the stator and rotor slot MMF harmonics, respectively, and the fourth term and fifth term are the air-gap field harmonics caused by the stator and rotor slot permeance harmonics.

B. Effect of Auxiliary Slot on Air-gap Magnetic Field

The auxiliary slots on the rotor side will change the amplitudes of permeance harmonics due to the opening of rotor slots and will double the spatial order of the permeance harmonics [15]. However, it can be seen from the equation (3)-(10) that this has no effect on the order and the amplitudes of the fundamental wave and harmonics of magnetomotive force. And it can be seen from the equation (15)-(18) that the auxiliary slots will change the amplitudes of permeance harmonics. This means that it mainly affects the fourth item on the right of equation (19), the air-gap field harmonics caused by the rotor slot permeance harmonics, which is obtained by multiplying the fundamental magnetomotive force and the rotor permeance harmonic.

The conventional method, which is shown in (15)-(18), can not calculate the permeance harmonics of the closed-slot motor. Therefore, it is necessary to establish the mathematical model to analyze the influence of auxiliary slots on rotor slot permeance harmonic.

III. Mathematical Ansys of Rotor Magnetic Conductivity Harmonic

This paper takes a 55 kW, 4-pole WSIM as the analysis object, which rotor has 42 slots. In order to simplify the analysis process, only 21 slots under a pair of poles are modeled.

A. Equivalent Slot Width

Considering that the slot bridge of the closed-slot motor is narrow and the flux density in the slot bridge is highly saturated, the Carter Factor needs to be corrected. A geometric method to calculate the equivalent slot opening of a closed-slot motor is proposed in the reference [21]

$$b_w=b_s-2h_{s0}\cot\alpha \tag{20}$$

where b_w is the equivalent slot opening, b_s is the slot width, h_{s0} is the slot bridge height, α is the inclined angle of the auxiliary line and α is adopted 45° in this paper.

B. Mathematical Model of Air-gap Permeance

To simplify the analysis, it is assumed that the stator side is not slotted and only the rotor side is slotted. Square waves are used to simulate the air-gap permeance, and the schematic is shown in Fig 1. The equivalent slot width of the auxiliary slot and the equivalent slot width of the rotor slot is calculated in the same way, and the air-gap permeability can be expressed as

$$\lambda_\delta=\frac{\mu_0}{\delta} \tag{21}$$

where $\mu_0=4\pi\times10^{-7}$ N/A^2 (T·m/A). δ is the length of air-gap.

For convenience of analysis, this paper uses the per unit model. The duty cycle of the square wave is obtained by the ratio of the equivalent slot width to the tooth pitch.

C. Size Optimization of Rotor Auxiliary Slot

When the auxiliary slot width is 2 mm, and the length is 9 mm, the mathematical model of air-gap permeance is shown in

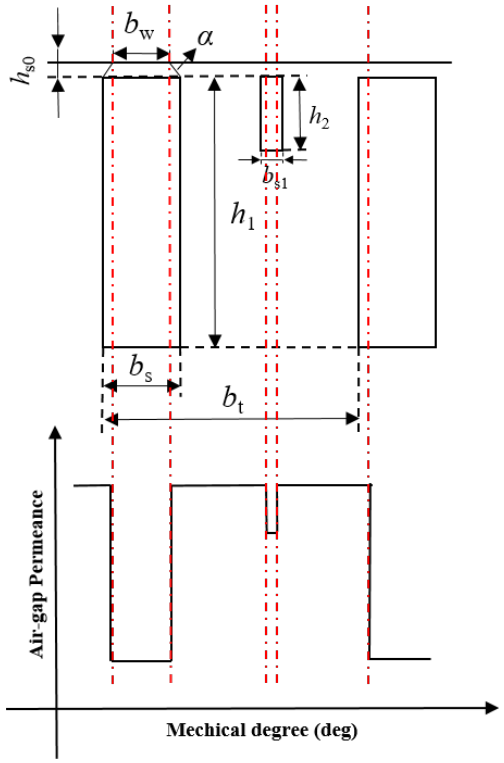

Fig. 1. Schematic diagram of the partial rotor of WSIM with auxiliary slot. Schematic diagram of mathematical model of air-gap permeance.

Fig 2. The Fourier decomposition of the air-gap permeance waveform is also shown in Fig 2. The fundamental component, 21st harmonic component, and 42nd harmonic component can be seen. Since there are 21 slots under a pair of poles of the rotor of the WSIM, these components correspond to the constant air-gap permeance part, the component of k_2=1, and the component of k_2=2 listed in (11)-(14), respectively. The latter two components produce the first-order and second-order rotor permeance harmonics under the action of fundamental magnetomotive force, respectively.

In order to analyze the effect of the auxiliary slot size on the rotor permeability harmonics, a parametric analysis of the length (h_2) and width (b_{s1}) of the auxiliary slot is required. After parametric analysis, the 21st and 42nd order components are extracted and plotted as Fig 3.

IV. Finite Element Validation

As shown in Fig. 4, the finite element model of the WSI with the auxiliary slots is established to further analyze the air-gap magnetic field, which is used to verify the method in section III, and all data of WSIM are listed in Table 1.

TABLE I
Initial Parameters of the Motor

Parameters	Value
Rated power (kW)	55
Rated voltage (V)	380
Frequency (Hz)	50
Number of poles pairs	2
Stator outer diameter (mm)	400
Stator inner diameter (mm)	225
Rotor inner diameter (mm)	85
Core length (mm)	180
Air-gap length (mm)	1

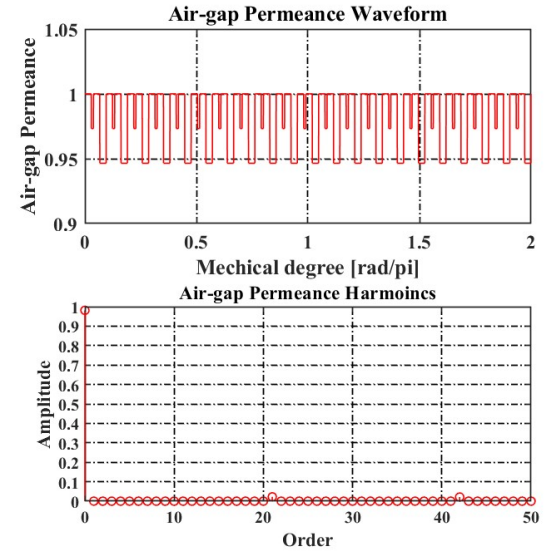

Fig. 2. Waveform diagram of air-gap permeance with auxiliary slot on rotor side. Harmonic of air-gap permeance with auxiliary slot on rotor side.

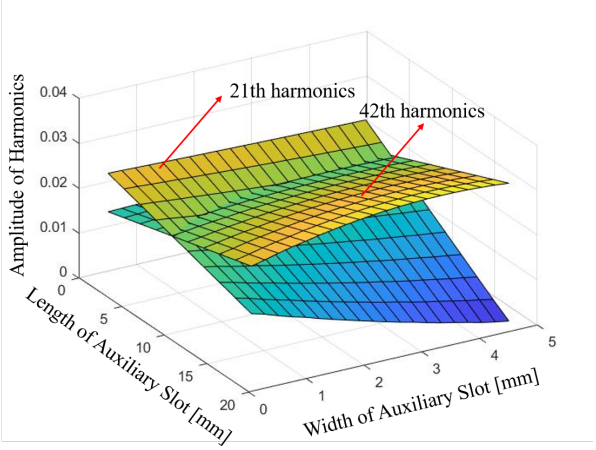

Fig. 3. Variation of harmonics of air-gap permeance with the size of auxiliary slot. Finite Element Simulation Model of WSIM

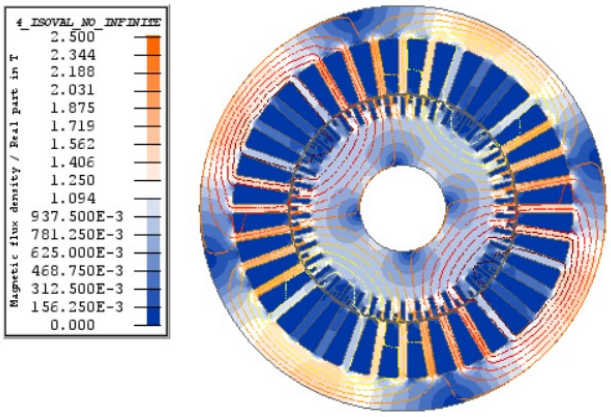

Fig. 4. The finite element simulation model of the motor with the Rotor Auxiliary Slot. The magnetic line of force of the motor is drawn and the magnetic density of the motor is marked.

The schematic diagram of the structure of the auxiliary slots is shown in Fig 5. As shown in Fig 5, three parameters are used to describe the position of the auxiliary slot. l_1 is used to indicate the width of auxiliary slots. l_2 is used to indicate the length of auxiliary slots. The motor rotor adopts a rectangular

slot which size is 4.7 mm* 18.7 mm, so the auxiliary slots of the rotor also adopted the rectangular slot.

Therefore, the value range of l_2 is 2.7- 4.7 mm, and the value range of l_3 is 2.7- 18.7 mm in the process of modeling the auxiliary slot. The initial value of l_3 is 1 mm, which is the same as the height of the slot bridge. The finite element simulation of the motor is carried out to solve the air-gap flux density, and the air-gap flux density is decomposed by the two-dimensional Fourier transform.

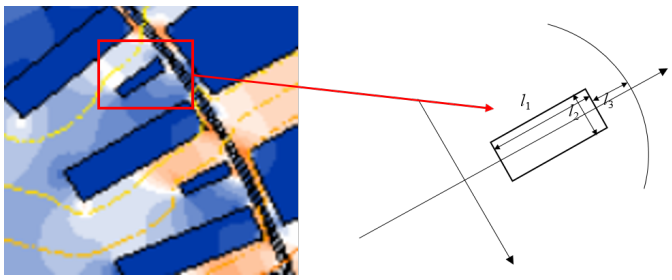

Fig. 5. The schematic diagram of the structure of the auxiliary slots

A. Rotor Permeance Harmonics

As shown in Fig.6, the harmonic content of the first-order rotor permeance harmonics of the motor decreases with the increase of the size of the auxiliary slots while the second-order rotor permeance harmonics keep almost remain. The weakening effect is more obvious when the width of the auxiliary slot is increased. At the same time, the saturation of tooth magnetic density is more serious.

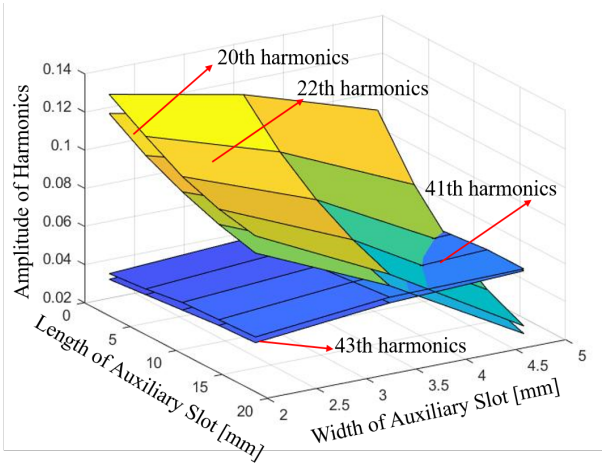

Fig. 6. Variation of harmonics of the air-gap flux density with the size of auxiliary slot.

V. Performance Analysis

A. THD of Air-gap Permance Waveform and Air-gap Flux Density Waveform

THD represents the sum of the square of the ratio of the effective value of the harmonic components, which order is less than H to the base wave component. The smaller the value of THD is, the better sinusoidal of the air gap magnetic field is. And the THD can be expressed as

$$\mathrm{THD}=\sqrt{\sum_{n=2}^{H}\left(\frac{G_n}{G_1}\right)^2} \tag{22}$$

where G_n is the effective value of the harmonic components, G_1 is the value of the base wave component, H is particular order of the harmonic. Since this paper mainly considers the 20th, 22th, 41th and 43th harmonic components, H is taken 50.

The total harmonic distortion (THD) of air-gap permeance waveform and air-gap flux density waveform are shown in Fig. 7 and Fig. 8. It can be seen that in the stage of small auxiliary slot size, the THD of both methods are decreasing, but with the increase of auxiliary slot size, the THD of both begins to increase. However, the minimum of the first is at the auxiliary groove size of 4.7* 10.7 mm^2, and the second is at 4.7* 14.7 mm^2.

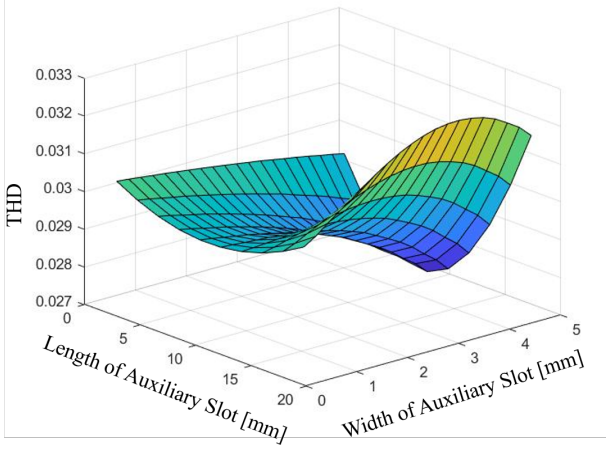

Fig. 7. THD of air-gap permeance waveform.

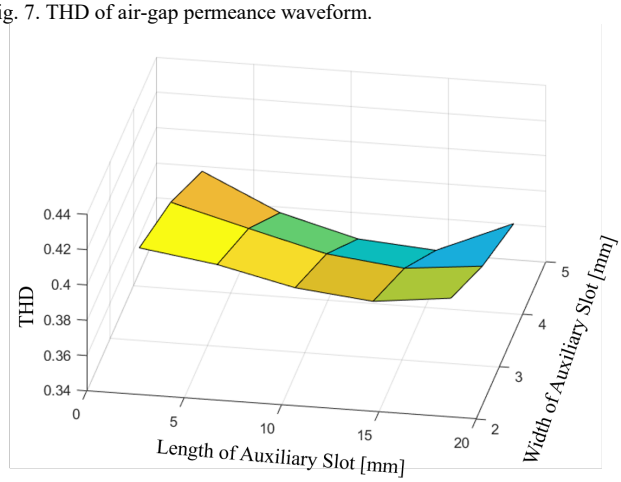

Fig. 8. THD of air-gap flux density waveform.

B. Comparison of the Radial Electromagnetic Force of Motor

The primary source of electromagnetic noise is manifested in the vibration of the stator and casing, and the main reason for the vibration of the stator and casing is the Maxwell radial force. The radial Maxwell force per unit area p_M at any location in the air gap can be calculated as

$$p_M(\theta,t)=\frac{b_r^2(\theta,t)-b_t^2(\theta,t)}{2\mu_0} \tag{23}$$

where θ is the mechanical angular position, μ_0 is the air-gap magnetic permeability, $b_r(\theta, t)$is the radial air-gap field, and $b_t(\theta, t)$is the tangential air-gap field. Cause of $b_r(\theta, t)$ is much bigger than $b_t(\theta, t)$, $b_t(\theta, t)$ is neglected in the following theoretical analysis in this paper, thus, equation (23) can be simplified as

$$p_{\mathrm{M}}(\theta,t)=\frac{b_r^2(\theta,t)}{2\mu_0} \tag{24}$$

where $b_{\mathrm{r}}(\theta, t)$ can be calculate as in (1).

In order to analyze the electromagnetic performance of WSIM brought by different sizes of the auxiliary groove, the finite element analysis model of different auxiliary sizes is established. WSIM. Then the radial Maxwell pressure is calculated according to the radial magnetic density of the motor as shown in (24). As shown in Fig. 9, after opening the auxiliary slots, the radial electromagnetic force of the motor was reduced by 28.4%.

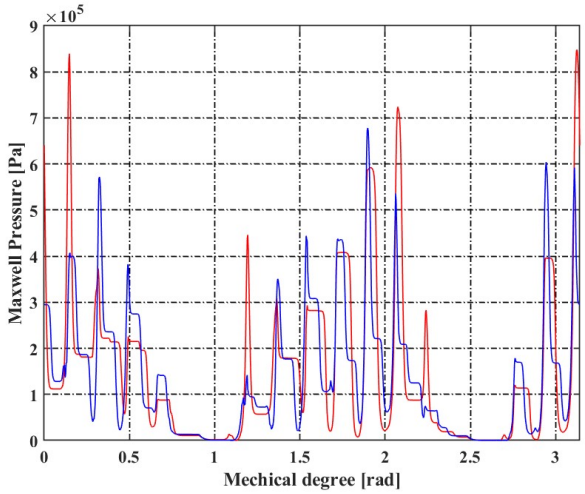

Fig. 9. Radial electromagnetic force of motor with and without auxiliary slot.

C. Comparison of Electromagnetic losses of Motor

The auxiliary slots will cause the saturation of the rotor tooth flux density, resulting in an increase in the motor loss. To further study the influence of auxiliary slots on the performance of the WSIM, the losses of the motors with different sizes of the auxiliary slots have been calculated.

During the simulation of the motors of different sizes of auxiliary slots, by changing the rotation rate of the motors, the output power of all the motors keep remain. The two-dimensional finite element calculation model of the motor is shown in Fig. 4.

Firstly the iron loss of submersible motors is calculated by the Bertotti iron loss model [22].

$$P_{\mathrm{Fe}}=k_h f B^{\alpha}+k_e f^2 B^2+k_{\alpha} f^{1.5} B^{1.5} \tag{25}$$

where f is frequency and B is magnetic flux density.

The coefficient k_{h}=248.549 $\mathrm{WsT^{-2}m^{-3}}$; k_{e}=1.506 $\mathrm{W(Ts^{-1})^{-3/2}m^{-3}}$; k_{α}=0 in the iron loss model were solved by curve fitting.

Secondly, the copper loss of the motors can be expressed as

$$P_{\mathrm{Cu}}=mI^2R_{\mathrm{AC}} \tag{26}$$

where m is the number of the phases, I is the current of a phase winding , R_{AC} is the AC resistance of a phase winding.

The AC resistance of a phase winding can be expressed as

$$R_{\mathrm{AC}}=k_{\mathrm{R}}\frac{Nl_{\mathrm{av}}}{\sigma S_{\mathrm{e}}} \tag{27}$$

where k_{R} is the coefficient of the resistance, N is the number of the turns, l_{av} is the average length of single turns, S_{c} is the cross-sectional area of the conductor, σ is the conductivity of the conductor.

The change of the copper losses and the iron loss with the auxiliary groove size is shown in Fig. 10, Fig. 11, and Fig. 12, respectively. The copper losses increase significantly with the size of the auxiliary groove, especially the stator copper loss, which is mainly because of the saturation of the rotor tooth part, which leads to the increased excitation current. Meanwhile, the iron loss of the motor decreases with increasing size because of the reduction in the harmonic content.

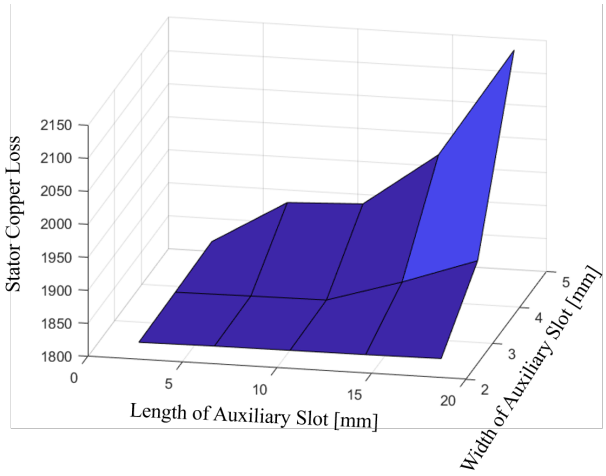

Fig. 10. The copper loss of the stator winding.

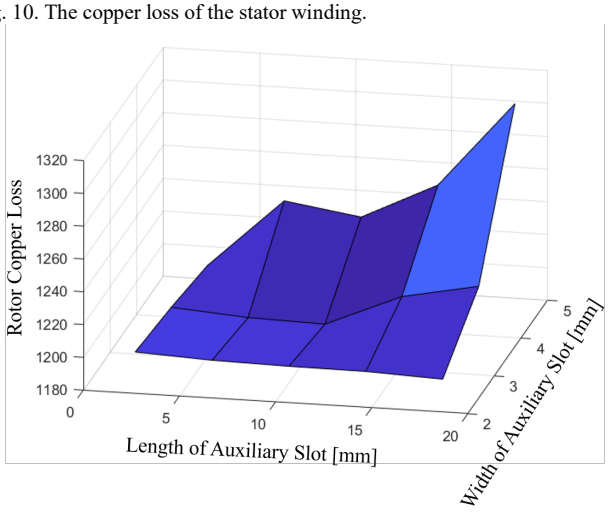

Fig. 11. The copper loss of the rotor bars and end rings.

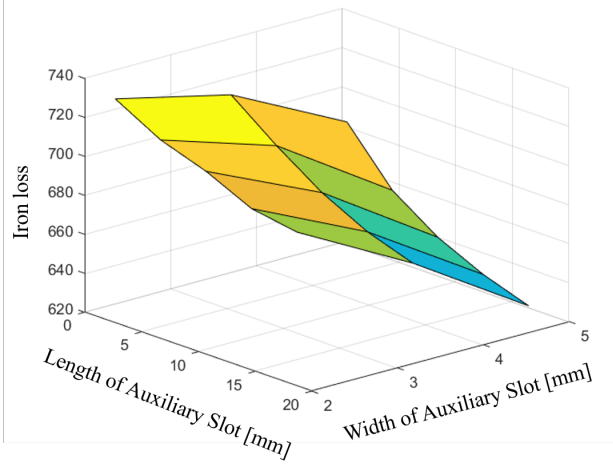

Fig. 12. The iron loss of the motor.

D. Comparison of the Magnetic Flux Density of the Rotor Tooth

The auxiliary slots on the rotor side will inevitably lead to the saturation of the rotor tooth flux density. Fig. 13 compares the magnetic density saturation of the rotor tooth with four different sizes of auxiliary slots. Fig. 13(a) and Fig. 13 (d) correspond to the motors with the minimum and maximum auxiliary groove size, respectively. Fig. 13(b) and Fig. 13(c) correspond to the motors, which auxiliary groove size is 4.7*10.7 mm^2 and 4.7*14.7 mm^2, respectively. It is obvious that the saturation degree of the motor tooth is also deepening with the increasing size of the auxiliary slots.

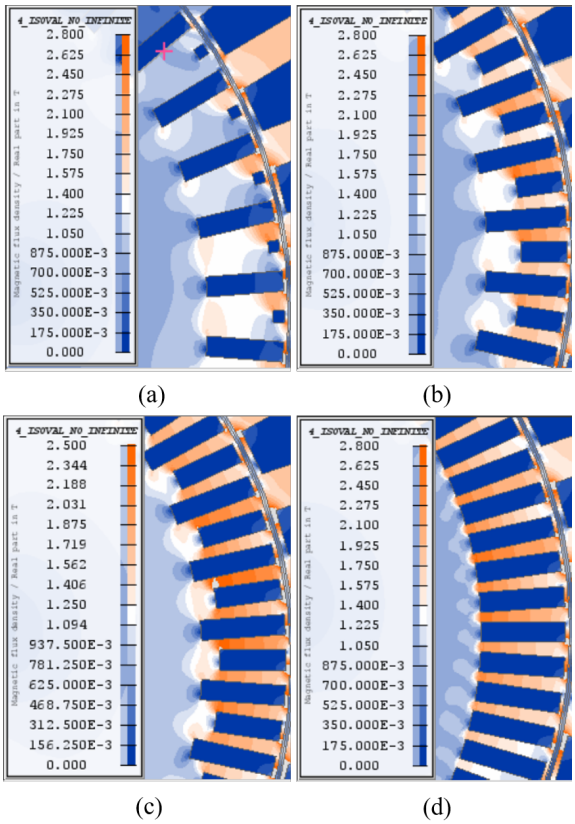

Fig. 13. The magnetic flux density of the motors with different size auxiliary slot.

E. Comparison of the Torque of the Motor

The output torque of the motor can be expressed as

$$T_2 = \frac{P_2}{\Omega} \tag{28}$$

where P_2 is the output power, Ω is the mechanical angular speed.

In this paper, the motor output power is guaranteed to be unchanged. Meanwhile, the slip of the motors change in a small range, so the change of the mechanical angular velocity is also small. In summary, the output torque of the motor remains almost constant. The torque changes of the motor with different sizes of auxiliary slots are shown in Fig. 14. As can be seen from Fig. 14, the torque almost dose not change with the size of the auxiliary slots. The difference between the maximum torque and the minimum torque is less than 5 N·m.

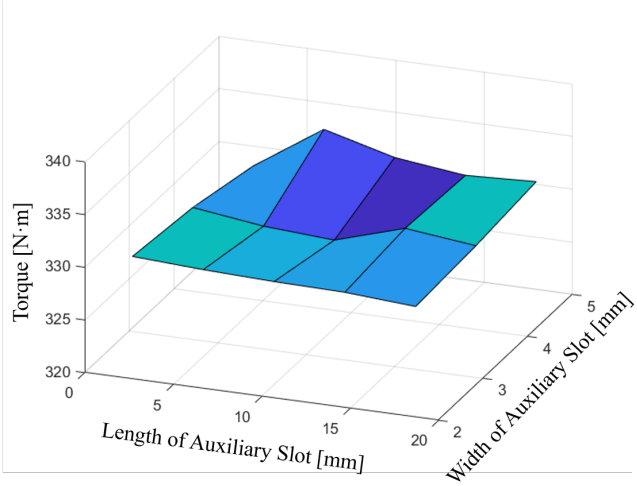

Fig. 14. The torque of the motor.

VI. Conclusion

Firstly, with the increase of auxiliary slots size, the first-order rotor permeance harmonics decreases while the second-order component increases, and the overall harmonic content decreases. Moreover, the analysis of the radial electromagnetic force of the motor also proves that the auxiliary slots can effectively reduce the electromagnetic vibration of the motor.

Secondly, the mathematical model presented in this paper can accurately analyze the variation of harmonics in the air-gap magnetic field with the size of the auxiliary slots. The method proposed in this paper fits well with the finite element simulation results.

Finally, as the size of the auxiliary groove increases, the saturation degree of the rotor tooth flux density is also getting higher and higher, which also leads to the increase of the current. And the increase of the current further leads to the increased copper loss of the motor. At the same time, with the increase of the motor auxiliary groove size, the harmonic content of the motor air gap magnetic field decreases, which reduces the harmonic loss of the motor. As for the torque performance of the motor, there is not much change.

References

[1] D. -J. Kim, J. -W. Jung, J. -P. Hong, K. -J. Kim and C. -J. Park, "A Study on the Design Process of Noise Reduction in Induction Motors," *IEEE Transactions on Magnetics*, vol. 48, no. 11, pp. 4638-4641, 2012.

[2] A.J. Ellison，S. J. Yang. "Natural Frequencies of Stators of Small Electric Machines," *Electrical Engineers*, vol. 118, no. 1, pp. 185-190, 1971.

[3] S. J. Yang. Low-noise electrical motors[M]. Oxford: Clarendon Press. 1981.

[4] F. Chai, Y. Li, Y. Pei, and Y. Yu, "Analysis of radial vibration caused by magnetic force and torque pulsation in interior permanent magnet synchronous motors considering air-gap deformations," *IEEE Transactions on Industrial Electronics*, vol. 66, no. 9, pp. 6703–6714, 2019.

[5] D. Kong, Z. Shuai, W. Li, and D. Wang, "Electromagnetic vibration characteristics analysis of a squirrel-cage induction motor under different loading conditions," *IEEE Access*, vol. 7, pp. 173 240–173 248, 2019.

[6] S. Sathyan, A. Belahcen, J. Kataja, T. Vaimann, and J. Sobra, "Computation of stator vibration of an induction motor using nodal magnetic forces," in *2016 XXII International Conference on Electrical Machines (ICEM)*, 2016, pp. 2198–2203.

[7] X. Guo, R. Zhong, M. Zhang, D. Ding and W. Sun, "Improved model of radial vibration in switched reluctance motor including magnetic saturation," *CES Transactions on Electrical Machines and Systems*, vol. 2, no. 4, pp. 363-370, 2018.

[8] D. Jiang, J. Chen and Z. Shen, "Common mode EMI reduction through PWM methods for three-phase motor controller," *CES Transactions on Electrical Machines and Systems*, vol. 3, no. 2, pp. 133-142, 2019.

[9] A. C. Binojkumar, B. Saritha and G. Narayanan, "Acoustic Noise Characterization of Space-Vector Modulated Induction Motor Drives—An Experimental Approach," *IEEE Transactions on Industrial Electronics*, vol. 62, no. 6, pp. 3362-3371, 2015.

[10] A. C. Binojkumar and G. Narayanan, "Variable switching frequency PWM technique for induction motor drive to spread acoustic noise spectrum with reduced current ripple," in *Proc. of 2014 IEEE International Conference on Power Electronics, Drives and Energy Systems (PEDES)*, 2014, pp. 1-6.

[11] H. Amlinger, I. Lopez Arteaga and S. Leth, "Impact of PWM switching frequency on the radiated acoustic noise from a traction motor," in *Proc. of 2017 20th International Conference on Electrical Machines and Systems (ICEMS)*, 2017, pp. 1-6.

[12] Y. Lu, J. Li, R. Qu, D. Ye, and H. Lu, "Electromagnetic force and vibration study on axial flux permanent magnet synchronous machines with dual three-phase windings," *IEEE Transactions on Industrial Electronics*, vol. 67, no. 1, pp. 115–125, 2020.

[13] Y. Lu, J. Li, R. Qu, D. Ye, H. Lu, J. Sun, M. Ge, and H. Xu, "Electromagnetic force and vibration analysis of permanent-magnet-assisted synchronous reluctance machines," *IEEE Transactions on Industry Applications*, vol. 54, no. 5, pp. 4246–4256, 2018.

[14] Y. Zhao, D. Li, T. Pei and R. Qu, "Overview of the rectangular wire windings AC electrical machine," *CES Transactions on Electrical Machines and Systems*, vol. 3, no. 2, pp. 160-169, 2019.

[15] G.-Y. Zhou and J.-X. Shen, "Rotor notching for electromagnetic noise reduction of induction motors," *IEEE Transactions on Industry Applications*, vol. 53, no. 4, pp. 3361–3370, 2017.

[16] X. Yongming, M. Dawei and W. Jiabin, "Numerical Calculation of End Leakage Reactance of Submersible Motor," in *Proc. of 2009 International Conference on Energy and Environment Technology, 2009*, pp. 184-188.

[17] H. Wang, X. Bao, C. Di, Z. Cheng and Y. Fang, "Current Analysis in End Ring of Submersible Motor by Finite-Element Method," in *Proc. of 2014 Fourth International Conference on Instrumentation and Measurement, Computer, Communication and Control*, 2014, pp. 983-987

[18] Wen Jiabin and Pan Yabin, "Research of six-pole permanent magnet submersible motor design," in *Proceedings of 2011 6th International Forum on Strategic Technology*, 2011, pp. 545-548.

[19] F. A. Gizatullin, M. I. Khakimyanov, F. F. Khusainov and I. N. Shafikov, "Analysis of losses in the cable line of well submersible electric motor," in *Proc. of 2017 International Conference on Industrial Engineering, Applications and Manufacturing (ICIEAM)*, 2017, pp. 1-3.

[20] A. Starikov, T. Tabachnikova and I. Kosorlukov, "Calculation of the Rotation Speed of a Submersible Induction Motor for the Tasks of Determining the Optimal Value of the Supply Voltage," in *Proc. of 2020 International Multi-Conference on Industrial Engineering and Modern Technologies (FarEastCon)*, 2020, pp. 1-4.

[21] X. Bao, N. Liang, Y. Fang, and F. Li, "Novel method of evaluation of carter factor for closed slot submersible motor including fringing effectand magnetic saturation," *Transactions of China Electrotechnical Society*, vol. 30, no. 12, pp. 220–227, 2015.

[22] F. Fiorillo and A. Novikov, "An improved approach to power losses in magnetic laminations under nonsinusoidal induction waveform," *IEEE Transactions on Magnetics*, vol. 26, no. 5, pp. 2904–2910, 1990.

Jiaxin Li (Non-member) was born in China. He received the B. Eng. Degree in Electrical Engineering and its Automation from Hefei University of Technology, Hefei, China, in 2019. He is currently working toward a master's degree in School of Electrical Engineering and Automation, Hefei University of Technology, Hefei, China.

His current research interests include motor design, finite-element analysis, and Simulation and analysis of the temperature field.

Jingwen Yan (Non-member) Her gotten the B.Eng. degree in material science from Soochow College, Suzhou, China, in 2018. She is right now seeking after the Ph.D. degree with the School of Electrical Designing and Computerization, Hefei College of Innovation, Hefei, China..

Her current research interests include motor electromagnetic design, iron loss calculation and analysis, motor harmonic analysis.

Chong Di (Non-member) was born in China. He received the B. Eng. and M. Eng. degrees from Hefei University of Technology, Hefei, China, in 2014 and 2017, respectively, and the Doctor of Science (D.Sc.) degree from Lappeenranta-Lahti University of Technology (LUT), Finland in 2020, all in electrical engineering. He is currently a researcher in the Department of Electrical Engineering, Hefei University of Technology, Hefei, China.

His research mainly concerns high-speed electrical machines and modelling of electrical machines on the open-source platform.

Xiaohua Bao (Member, IEEE) was born in China. He received his B.Eng., M.Eng., and Ph.D. degrees in electrical engineering from the Hefei University of Technology, Hefei, China, in 1996, 2002, and 2008, respectively. He joined the School of Electrical Engineering and Automation, Hefei University of Technology, where he became a Professor in 2012. He was a Visiting Scholar with the Virginia Polytechnic Institute and State University, Blacksburg, VA, United States.

His current research interests include motor design, magnetic field analysis, and finite-element analysis.

Qinglong Zhu (Non-member) was born in China. He received the B. Eng. Degree in Electrical Engineering and its Automation from Hefei University of Technology, Hefei, China, in 1982. He is currently the chairman of Hefei Hengda Jianghai Pump Co., Ltd, Hefei, China.

His current research interests include the electric pump technology of the large diving motor and the integrated automation system of the pump station.